^{18}F-FDG Labeling of Mesenchymal Stem Cells and Multipotent Adult Progenitor Cells for PET Imaging: Effects on Ultrastructure and Differentiation Capacity

Esther Wolfs[1], Tom Struys[2,3], Tineke Notelaers[4], Scott J. Roberts[5], Abhishek Sohni[4], Guy Bormans[6], Koen Van Laere[1], Frank P. Luyten[5], Olivier Gheysens[1], Ivo Lambrichts[2], Catherine M. Verfaillie[4], and Christophe M. Deroose[1]

[1]Division of Nuclear Medicine and Molecular Imaging, Department of Imaging and Pathology, KU Leuven, Leuven, Belgium; [2]Lab of Histology, Department of Functional Morphology, Biomedical Research Institute, Universiteit Hasselt, Diepenbeek, Belgium; [3]Biomedical NMR Unit, Department of Imaging and Pathology, KU Leuven, Leuven, Belgium; [4]Stem Cell Institute, Department of Development and Regeneration, KU Leuven, Leuven, Belgium; [5]Laboratory for Skeletal Development and Joint Disorders, KU Leuven, Leuven, Belgium; and [6]Laboratory for Radiopharmacy, KU Leuven, Leuven, Belgium

Because of their extended differentiation capacity, stem cells have gained great interest in the field of regenerative medicine. For the development of therapeutic strategies, more knowledge on the in vivo fate of these cells has to be acquired. Therefore, stem cells can be labeled with radioactive tracer molecules such as ^{18}F-FDG, a positron-emitting glucose analog that is taken up and metabolically trapped by the cells. The aim of this study was to optimize the radioactive labeling of mesenchymal stem cells (MSCs) and multipotent adult progenitor cells (MAPCs) in vitro with ^{18}F-FDG and to investigate the potential radiotoxic effects of this labeling procedure with a range of techniques, including transmission electron microscopy (TEM). **Methods:** Mouse MSCs and rat MAPCs were used for ^{18}F-FDG uptake kinetics and tracer retention studies. Cell metabolic activity, proliferation, differentiation and ultrastructural changes after labeling were evaluated using an Alamar Blue reagent, doubling time calculations and quantitative TEM, respectively. Additionally, mice were injected with MSCs and MAPCs prelabeled with ^{18}F-FDG, and stem cell biodistribution was investigated using small-animal PET. **Results:** The optimal incubation period for ^{18}F-FDG uptake was 60 min. Significant early tracer washout was observed, with approximately 30%–40% of the tracer being retained inside the cells 3 h after labeling. Cell viability, proliferation, and differentiation capacity were not severely affected by ^{18}F-FDG labeling. No major changes at the ultrastructural level, considering mitochondrial length, lysosome size, the number of lysosomes, the number of vacuoles, and the average rough endoplasmic reticulum width, were observed with TEM. Small-animal PET experiments with radiolabeled MAPCs and MSCs injected intravenously in mice showed a predominant accumulation in the lungs and a substantial elution of ^{18}F-FDG from the cells. **Conclusion:** MSCs and MAPCs can be successfully labeled with ^{18}F-FDG for molecular imaging purposes. The main cellular properties are not rigorously affected. TEM confirmed that the cells' ultrastructural properties are not influenced by ^{18}F-FDG labeling. Small-animal PET studies confirmed the intracellular location of the tracer and the possibility of imaging injected prelabeled stem cell types in vivo. Therefore, direct labeling of MSCs and MAPCs with ^{18}F-FDG is a suitable technique to noninvasively assess cell delivery and early retention with PET.

Key Words: mesenchymal stem cell; multipotent adult progenitor cell; ^{18}F-FDG; radiotoxicity; PET

In the last few decades, adult stem cells have gained interest because they possess great potential for tissue engineering and regenerative medicine, with limited ethical concerns regarding their use (*1,2*). Nearly all human tissues contain a source of adult stem cells, where they function in tissue repair after injury or for natural tissue turnover. Depending on their origin, these cells possess the ability to differentiate into a variety of cell types of the body.

Mesenchymal stem cells (MSCs) are self-renewing multipotent stem cells that were first isolated from bone marrow (*3*); however, other body tissues such as muscle (*4*), adipose tissue, (*5*) and dental pulp (*6*) were also proven to contain a population of MSCs. These cells have the ability to differentiate into different cell types along the mesenchymal lineage, with the ability to form bone, cartilage, and adipose tissue (*7,8*). They appear to be good candidates for clinical use, because they can be expanded easily in vitro and they lack immunogenicity, and they have significant trophic effects on endogenous (stem) cells. Furthermore, MSCs possess immunity-modulating properties, through the inhibition of immune cell function and proliferation, and their use as immunomodulators is being explored clinically (*9*).

Multipotent adult progenitor cells (MAPCs) may represent another clinically useful source of adult stem cells.

MAPCs have been isolated from mouse, rat, and human bone marrow cells and from murine muscle and brain (*10,11*). In contrast to MSCs, they have broader differentiation ability; in rats, for instance, they differentiate into various cell types of the 3 different germ layers, including endothelial cells, smooth muscle cells, osteoblasts, adipocytes, hepatocytes, and neural stem cell-like cells (*12,13*). Additionally, MAPCs have immune modulatory properties similar to MSCs (*11*).

Several preclinical studies have already shown the positive effects of grafted stem cells on the repair and regeneration of various tissues in vivo, such as bone (*14*), cartilage (*15*), and myocardium (*16*). Additionally, MSCs and MAPCs injected intravenously have been shown to home to tumors in vivo, making them potential vehicles for anticancer therapy (*17,18*). Moreover, both MSCs and MAPCs have gained interest for in vivo applications because of their immunomodulatory properties (*11*), and both cell types are being tested in phase I and II clinical studies. Together with the development of new stem cell–based therapeutic approaches, the search for effective and noninvasive imaging techniques for stem cell tracking in vivo is crucial. In vivo imaging can provide information on cell biodistribution, quantification of targeted cells, in situ persistence, survival, and function (*19*).

Nuclear imaging modalities such as PET can serve as noninvasive, sensitive, quantitative, and longitudinal approaches for in vivo stem cell tracking. Stem cells can be labeled with low doses of radioactive tracer molecules and detected on decay. ^{18}F-FDG has been used for the imaging of initial stem cell biodistribution after injection into subjects (*20*).

^{18}F-FDG has already been used to image different cell types, such as dendritic cells, bone marrow–derived cells, or hematopoietic stem cells, both in preclinical models and in humans (*21–23*). However, the effects of labeling stem cells with ^{18}F-FDG have not been extensively studied with respect to their function and viability.

The aim of this study was thus to optimize and characterize radiolabeling of MSCs and MAPCs with ^{18}F-FDG. We performed a thorough examination of stem cell properties and function after labeling and presented for the first time, to our knowledge, data on electron microscopic assessment of labeling-induced morphologic changes

MATERIALS AND METHODS

Cell Culture

MSCs and MAPCs were kept in culture as previously described (*13*). For a more detailed description, we refer the reader to the supplemental data (supplemental materials are available online only at http://jnm.snmjournals.org).

Radiolabeling Optimization

For radiolabeling experiments, 100,000 cells were seeded per well in a 24-well plate. Cells were incubated in culture medium until attachment to the surface occurred. Subsequently, MSCs and MAPCs were washed with phosphate-buffered saline (PBS; Gibco) and incubated with a 0.74 MBq/mL solution of ^{18}F-FDG in glucose-free Dulbecco modified Eagle medium (Gibco) at 37°C. After incubation, cells were washed 3 times with PBS, and tracer concentration in the cell fraction was measured using a γ-counter (Perkin Elmer).

For uptake kinetics assessment (*n* = 6), cells were incubated with ^{18}F-FDG for different periods (5, 15, 30, 45, 60, 90, 120, 150, 180, 210, 240, 270, 300, and 360 min). Cellular tracer concentration was similarly measured after each time point.

Tracer washout was measured by incubation of cells as described above for 1 h, followed by 3 PBS washes and a second incubation on cold PBS for different periods (0, 5, 15, 30, 60, 90, 150, and 180 min). Cellular tracer concentration was similarly measured after each time point (*n* = 6).

In Vitro Toxicity Assays

For the determination of tracer radiotoxicity on MSCs and MAPCs, cells were seeded and incubated with a 0.74 MBq/mL solution of ^{18}F-FDG in glucose-free Dulbecco modified Eagle medium at 37°C for 30, 60, 90, 120, and 180 min. Different cell type–specific properties were assessed, such as cell proliferation, cell metabolic activity, differentiation capacity, and ultrastructural properties (*n* = 3).

Cell Proliferation. The effect of radiolabeling on cell proliferation was assessed for 10 d by determining cell doubling times (DTs), calculated from cell counts and interpassage time according to the following formulas (*24*):

$$CD = \ln(Nf/Ni)/\ln(2)$$

$$DT = CT/CD,$$

where CT is the interpassage period, CD the cell doubling number, Nf the number of calculated cells at the end of passage x, and Ni the initial number of seeded cells for passage x. Data are presented as DT values relative to unlabeled control cells.

Cellular Metabolic Activity. Cell metabolic activity after radiolabeling was measured using the Alamar Blue (Invitrogen) reagent. After radiolabeling, cells were seeded, and 10% of Alamar Blue was added to the culture medium for 2 h at 37°C. Fluorescence was measured at an excitation wavelength of 570 nm, with an emission of 585 nm in a Victor 1420 plate reader (Perkin Elmer). The effect on cell metabolism was monitored for 10 d, and data are presented as values relative to unlabeled control cells.

MSC and MAPC Differentiations. Information about MSC and MAPC differentiation is given in the supplemental data.

Ultrastructural Analysis. The effects of labeling MSCs and MAPCs with ^{18}F-FDG on the ultrastructure of the cells were evaluated after labeling cells for 30, 60, 90, 120, and 180 min. Cells were seeded on Thermanox slides (Nunc), labeled with ^{18}F-FDG for different time points, and fixed with 2% glutaraldehyde in 0.05 M sodium cacodylate buffer after 180 min. After fixation, cells were fixed in 2% osmium tetroxide for 1 h and stained with 2% uranyl acetate in 10% acetone for 20 min. Subsequently, the cell-seeded coverslips were put through a dehydrating series of graded concentrations of acetone and embedded in araldite according to the pop-off method (*25*). Ultra-thin sections (60 nm) were mounted on 0.7% formvar-coated grids (Wacker), contrasted with uranyl acetate and lead citrate, and examined with a Philips EM 208 transmission electron microscope operated at 80 kV. Digital images were captured using a Morada camera system (Olympus).

For quantification purposes, images were analyzed using SIS software. Random images were taken, and the following parameters were examined for each labeling condition: number of vacuoles per cell, number of lysosomes per cell, average lysosome size, mitochondrial length, and narrowest rough endoplasmic reticulum (rER) width.

Small-Animal PET Scans of ^{18}F-FDG–Labeled Cells

Cells (100,000/well) were seeded in a 24-well plate. After attachment to the surface, cells were labeled in vitro for 60 min with ^{18}F-FDG (0.74 MBq/mL). Cells were washed 3 times with PBS, harvested, and injected in the lateral tail vein of healthy mice, according to the guidelines from the local animal ethical committee. Animals were brought under anesthesia with 2% isoflurane (Isoflurane USP; Rothacher Medical) in 100% oxygen, at a flow rate of 2 L/min. A 2-h dynamic small-animal PET scan was acquired for the generation of time–activity curves ($n = 3$/cell type). Also, 10 min after injection a 20-min static scan was obtained ($n = 3$/cell type). Imaging was performed on a Focus 220 microPET system (Siemens Medical Solutions USA). Images were reconstructed with a filtered backprojection algorithm and analyzed in PMOD (PMOD Technologies). Images were converted to standardized uptake value according to the following standard formula: standardized uptake value = (activity concentration in organ)/[(activity injected)/(weight of animal)]. The total fraction of injected activity in the lungs was calculated using a manually delineated volume of interest. A volume of interest was positioned on the dynamic images around the lungs, brain (as a control organ for the uptake of eluted ^{18}F-FDG), and bladder to generate time–activity curves.

Statistical Analysis

Data are given as mean ± SD. All datasets were first checked for normal distribution using the Kolmogorov–Smirnov test. ANOVA statistical tests were performed with Tukey post hoc tests. P values of less than 0.05 were considered statistically significant. Data were processed using Prism (version 5.00; GraphPad Software) for Windows (Microsoft).

RESULTS

Radiolabeling Optimization

First, MSCs and MAPCs were incubated with ^{18}F-FDG for different periods to assess the uptake kinetics (Fig. 1A). For MAPCs, experiments showed a continuously increasing decay-corrected uptake, with longer incubation periods up to 6 h. For MSCs, a similar increase was seen, with a leveling of the slope after 210 min. The optimal incubation period for labeling cells with ^{18}F-FDG was determined to be 60 min when absolute radioactivity levels (without decay correction) were taken into account (Fig. 1B).

After MSCs and MAPCs were radiolabeled with ^{18}F-FDG for 60 min, a significant ^{18}F-FDG elution could be detected, decreasing progressively within the first 120 min (Fig. 1C). Approximately 30% and 40% of the initially incorporated ^{18}F-FDG was trapped inside the MSCs and MAPCs, respectively, after 3 h.

In Vitro Toxicity Assays

Cell Proliferation. The effect of ^{18}F-FDG labeling on cell proliferation was assessed for 10 d after labeling by calculating the DTs relative to unlabeled control cells.
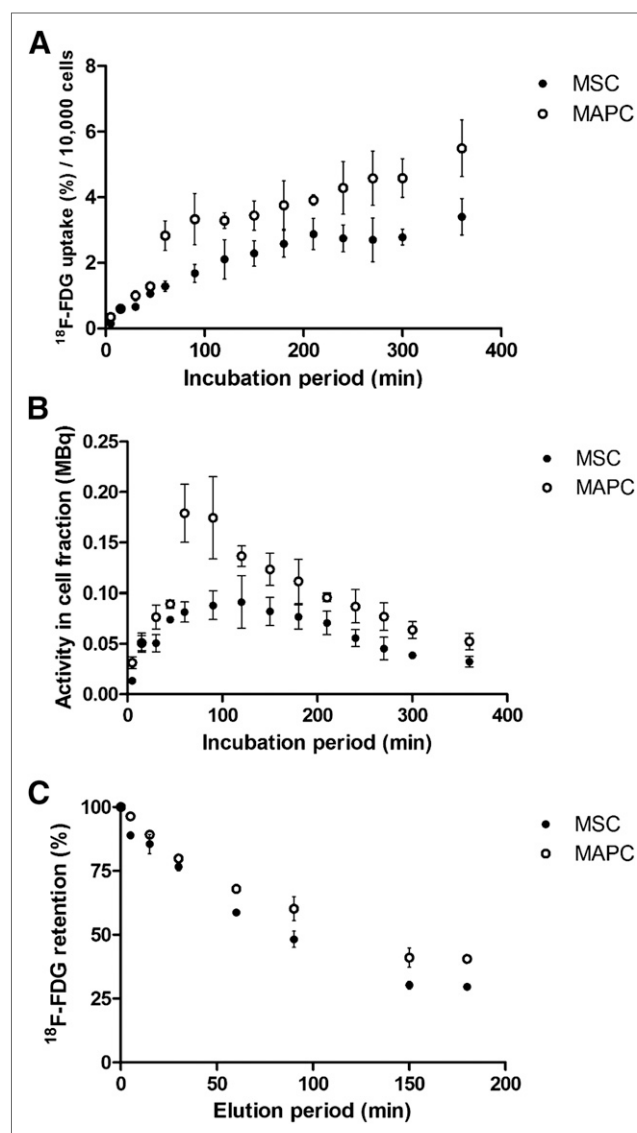

FIGURE 1. (A and B) ^{18}F-FDG uptake kinetics in MSCs and MAPCs: data corrected for radioactive decay (A) and uncorrected data (B). (C) Cellular retention of incorporated ^{18}F-FDG within 180 min.

MSCs and MAPCs labeled for 180 min showed a significant increase in DT (Supplemental Fig. 1). For MSCs, the proliferation of cells labeled for 180 min was significantly impaired on day 2 ($P < 0.05$). An increase in cell proliferation ($P < 0.05$) was observed for all other labeling conditions on day 2. Proliferation rates recovered to normal values in all conditions by day 4.

For MAPCs, labeling cells for 180 min caused a significantly reduced proliferation rate on days 1 and 2 ($P < 0.01$). All other labeling conditions demonstrated a moderately enhanced proliferation capacity on day 2 after labeling ($P < 0.05$). Both effects disappeared on day 4, when all labeled cells showed proliferation rates similar to control cells.

Cellular Metabolic Activity. After MSCs and MAPCs were labeled with ^{18}F-FDG, cell metabolism was monitored for 10 d (Supplemental Fig. 2). On day 1, cells labeled for
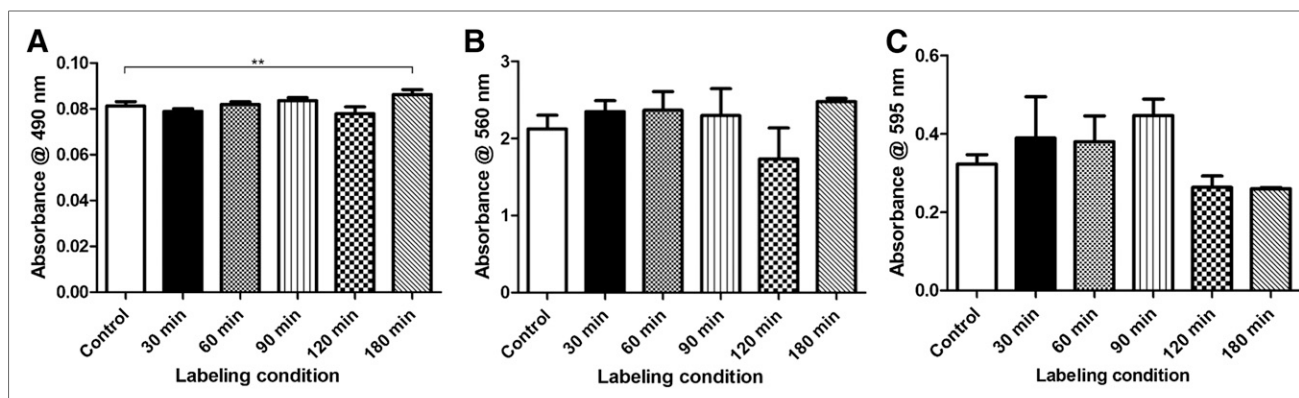
FIGURE 2. Adipogenic, osteogenic, and chondrogenic differentiations of MSCs labeled with ^{18}F-FDG. (A) Extraction of Oil red O dye after adipogenic differentiation measured at 490 nm. (B) Extraction of Alizarin red S (Sigma-Aldrich) dye from differentiated osteoblasts, measured at 560 nm. (C) Extraction of Alcian Blue (Sigma-Aldrich) dye from differentiated chondrocytes, measured at 595 nm. **$P < 0.01$.

60 min showed an increased metabolic activity relative to control cells ($P < 0.01$). No significant differences in cell metabolism could be detected on other days after labeling.

For MAPCs, ^{18}F-FDG labeling also led to an increase in day 1 metabolic activity within cells labeled for 30 min ($P < 0.01$). On day 2 after labeling, a significantly decreased metabolic activity was observed in cells labeled for 30, 90, 120, and 180 min ($P < 0.05$). This effect recovered to normal values after further follow-up.

MSC Differentiation. MSCs labeled with ^{18}F-FDG for different periods all showed adipogenic differentiation capacity (Supplemental Fig. 3A; representative image for all conditions). Fat droplets were stained using the Oil red O solution (Sigma-Aldrich), and quantification of the extracted dye showed only minor effects of the labeling (Fig. 2A). The only significant difference between control cells and labeled cells was for MSCs incubated for 180 min with ^{18}F-FDG, which demonstrated a small increase in fat-droplet staining of 6%, compared with control cells ($P < 0.01$). However, this small increase is probably not biologically relevant.

After osteogenic differentiation, matrix mineralization could be stained using alizarin red S in all conditions (Supplemental Fig. 3B; representative image for all conditions). Extraction of the dye also did not indicate a statistical difference between labeling conditions, compared with control cells (Fig. 2B). Alkaline phosphatase activity did not differ significantly in any conditions (Supplemental Fig. 3C).

Chondrogenic differentiation was confirmed with an immunostaining for aggrecan (Supplemental Fig. 3D and Supplemental Table 2; all primary antibodies used in this study). Alcian blue staining showed the production of an immature chondrogenic matrix of glycosaminoglycans and mucopolysaccharides (Supplemental Fig. 3E; representative images). No statistical difference in alcian blue dye incorporation within the chondrogenic micromasses was observed between the different labeling conditions (Fig. 2C).

MAPC Differentiation. We also assessed the hepatic differentiation of MAPCs incubated with ^{18}F-FDG for different time periods, using quantitative real-time polymerase chain reaction and immunostaining. For all genes tested, no significant differences in gene expression pattern or levels could be observed between the tested labeling conditions (Supplemental Figs. 4A–4C). Transcripts for both mature (*Alb, G6P*) and immature (*Hnf4α, Afp*) hepatic gene markers were induced in all conditions.

To further confirm the differentiation of labeled MAPCs toward the hepatic lineage, immunofluorescence was performed for the nuclear protein Hnf4α and the cytoplasmic protein albumin (Supplemental Fig. 4D). Both proteins proved to be present, with albumin more abundant than Hnf4α.

Smooth-muscle differentiation was induced after labeling MAPCs with ^{18}F-FDG by exposing the cells to transforming growth factor β and platelet-derived growth factor-BB. Gene expression patterns were checked by quantitative real-time polymerase chain reaction on sequential days, and no significant differences were observed in expression pattern or levels for any of the marker genes tested (Supplemental Figs. 4E–4G). Transcripts for both early marker genes (Sm22α) and mature marker genes ([1]H-calponin, SMαactin) were expressed in all conditions. Immunofluorescence also confirmed these data, with a positive staining for Sm22α (Supplemental Fig. 4H), [1]H-calponin, and SMαactin (data not shown).

After ^{18}F-FDG labeling, MAPCs were exposed to a neuroectodermal differentiation protocol. Differentiation to immature neuroprogenitors, as previously described, was seen for all MAPC populations (*11*). This differentiation was exemplified by a significant decrease of the pluripotency marker Oct4 and an increase of the neuroectodermal marker transcripts *Pax6* and *Sox2* (Supplemental Figs. 4I–4K).

Ultrastructural Analysis. We also evaluated the ultrastructural characteristics of MSCs labeled with ^{18}F-FDG (Fig. 3A). The following different parameters were examined
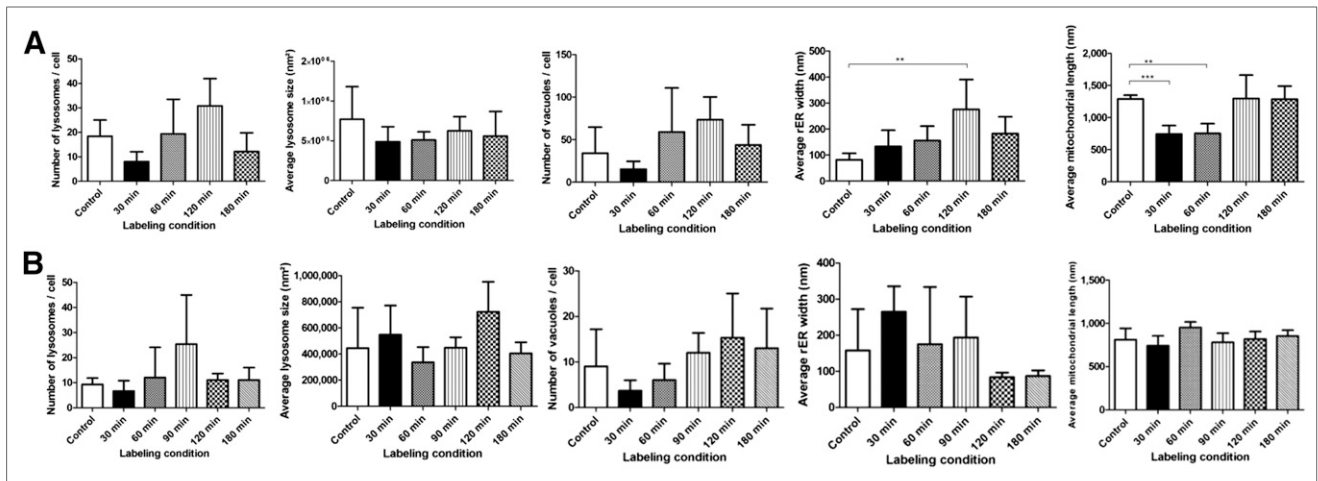
FIGURE 3. Quantitative data from TEM of MSCs (A) and MAPCs (B). For both cell types, the following different parameters were assessed: number of lysosomes per cell, average lysosome size, number of vacuoles per cell, average rER width, and average mitochondrial size.

within randomly taken images: number of lysosomes per cell, average lysosome size, number of vacuoles per cell, average narrowest rER width, and average mitochondrial length. A significantly dilated rER width was observed within cells labeled for 120 min ($P < 0.05$). Furthermore, the mitochondrial length was significantly shorter in MSCs labeled for 30 and 60 min ($P < 0.01$).

The effect of radiolabeling with ^{18}F-FDG on the ultra-structure was also evaluated in MAPCs (Fig. 3B). No significant differences were present in any of the conditions for any tested parameter.

Small-Animal PET Scans of ^{18}F-FDG–Labeled Cells

MSCs and MAPCs labeled for 60 min with ^{18}F-FDG before intravenous injection were imaged using small-animal PET (Fig. 4). The lungs contained 52% and 43% of the total injected activity for MSCs (Fig. 4A) and MAPCs (Fig. 4C), respectively.

Furthermore, dynamic 2-h small-animal PET data acquisitions (Figs. 4B and 4D) show a gradual signal reduction in Bq/cm^3 in the lungs, along with a gradual signal increase in the bladder. For MSCs and MAPCs, respectively, 59% and 32% of the highest pulmonary signal was
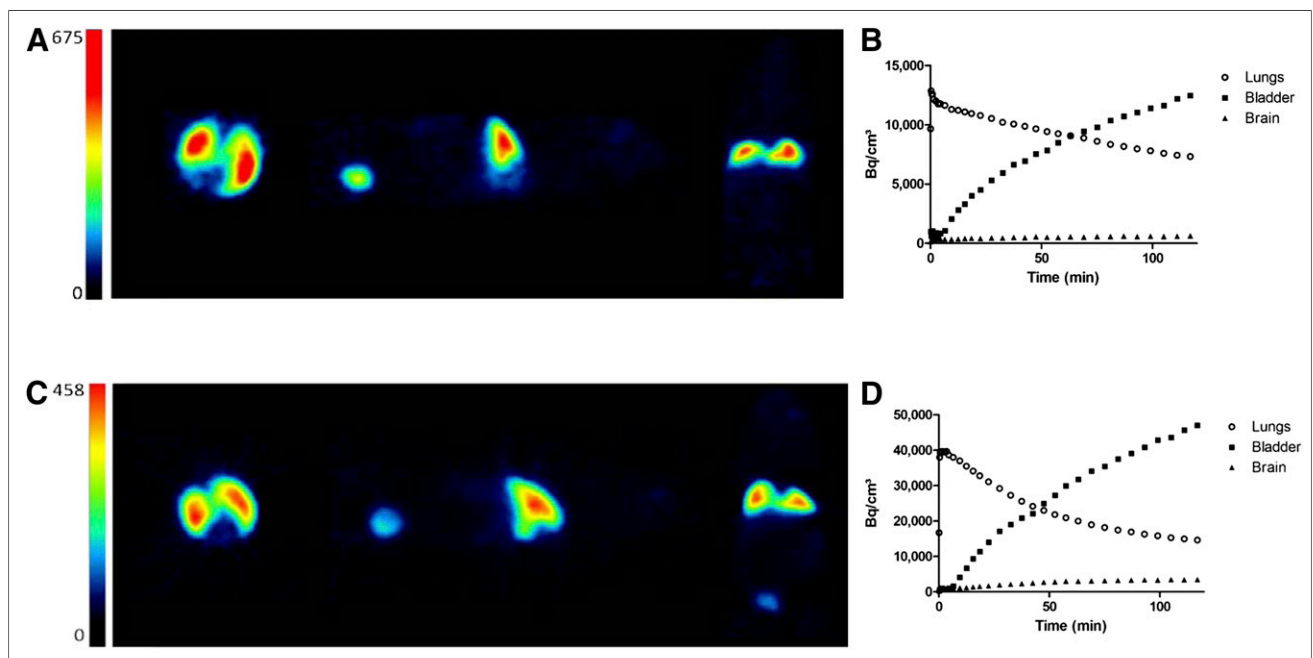
FIGURE 4. Small-animal PET data of injected MSCs (A–B) and MAPCs (C–D) labeled with ^{18}F-FDG. Dynamic data from lungs and bladder suggest in vivo elution of ^{18}F-FDG from cells for both cell types. Brain dynamic data were included as control for free ^{18}F-FDG uptake ($n = 500,000$).

retained in the lungs after 2 h. The signal in the brain was also assessed as a control for the uptake of eluted ^{18}F-FDG in the body, and this signal remained low during the scan.

DISCUSSION

Stem cell–based therapies are currently being explored in the setting of tissue engineering and regenerative medicine. Understanding the behavior of cells within the human body is of importance for the development of these new and advanced medicinal therapeutic products. Noninvasive imaging methods can provide invaluable information on the fate of the cells at different time points. Labeling stem cells with radioactive tracer molecules for PET imaging is a suitable method for these purposes.

In this study, MSCs and MAPCs were labeled with ^{18}F-FDG, a glucose-analog, which is metabolically trapped inside cells after phosphorylation by hexokinase. ^{18}F-FDG can be produced at acceptable costs and is readily available because of its widespread clinical use (23). Furthermore, ^{18}F-FDG has already been used to image stem cells administered to patients (23). However, when labeling cells for noninvasive detection, the tracer should not or only minimally affect the function and biologic properties of the labeled cells. Herein, MSCs and MAPCs were labeled with ^{18}F-FDG in various conditions, and the effect on cellular properties and their biologic behavior was evaluated.

First, tracer uptake kinetics was assessed. A more or less linear relationship between incubation time and ^{18}F-FDG uptake was observed. By taking decay into account, the optimal incubation period for both MSCs and MAPCs with ^{18}F-FDG was assessed at 60 min.

An important drawback, however, was the relatively high tracer elution from the cells. Three hours after labeling, approximately 30% of the intracellular ^{18}F-FDG was retained within the cells (Fig. 2). This retention has also been reported by other groups, in different cell types. Doyle et al. have shown an ^{18}F-FDG washout of 30%–40% from labeled circulating progenitor cells (26). Melder et al. demonstrated an elution of 21% of the ^{18}F-FDG from IL-2–activated natural killer cells (27). Furthermore, a study by Adonai et al. confirmed these data, with an efflux of 63% from C6 rat glioma cells after 5 h (28). This efflux is possibly caused by the high load of ^{18}F-FDG within the cells, which cannot be entirely phosphorylated by hexokinase, and hence, the nonmetabolized tracer molecules can diffuse back out of the cell. Despite the high efflux of ^{18}F-FDG that was reported in various studies, it was feasible to acquire PET images and to depict the presence of labeled cells in the body. The eluted activity from the cells in vivo will therefore not be sufficient to cause a significant background signal because the eluted ^{18}F-FDG molecules will be only partly taken up by the surrounding tissue. The other molecules will enter the bloodstream and will be distributed throughout the body. Therefore, the eluted ^{18}F-FDG molecules will not concentrate in a single tissue or organ, except for the urinary system and the bladder for excretion.

Consequently, the signal in nontarget tissue will be low, thus enabling the imaging of cell delivery and early retention.

We noted an effect of labeling with ^{18}F-FDG on both MSC and MAPC proliferation, although the effect was transient. Conversely, no effect of ^{18}F-FDG labeling on metabolic activity in the days after labeling was observed in MSCs and MAPCs using Alamar Blue (Invitrogen), a cell-permeable compound (resazurin) that is converted to a fluorescent compound (resorufin) by metabolically active cells. Our results are in line with those of Elahmi et al., who labeled adipose-derived stem cells for 90 min with amounts of ^{18}F-FDG ranging between 0 and 7.4 MBq. After ^{18}F-FDG labeling, a delay in adipose-derived stem cell proliferation was observed without changes in viability (29).

Furthermore, the respective differentiation abilities of MSCs and MAPCs labeled with ^{18}F-FDG were assessed. No significant effect on the ability of MSC to differentiate to adipocytes, chondrocytes, and osteoblasts was found. Likewise, we could not detect an effect of the labeling on the ability of MAPC to generate smooth muscle cells, hepatocytelike cells, and neuroprogenitorlike cells. Chen et al. also showed a preserved differentiation capacity in human MSCs after external-beam irradiation up to 9 Gy, which is a high effective dose (30). Conversely, Elhami et al. found a reduced adipogenic differentiation capacity after ^{18}F-FDG labeling in adipose-derived stem cells labeled with 3.7 MBq for 90 min (29).

We also evaluated the effect of radiolabeling on the cellular ultrastructure using transmission electron microscopy. No significant changes were observed in the ultrastructure of the MAPCs after labeling with ^{18}F-FDG. By contrast, some differences were detected in MSCs after labeling with ^{18}F-FDG: decreased size of mitochondria and dilated rER. The average mitochondrial length in labeled MSCs was significantly reduced after labeling for 30 and 60 min. This effect can be attributed to the dynamics of natural mitochondrial fusion and fission for normal respiratory function in mammalian cells (31,32). After MSCs were labeled for 120 min, the rER width was significantly larger. The rER serves as an environment for protein maturation and folding. Unfolded or damaged proteins will be stacked inside the rER lumen, with an rER dilation as a consequence (33). These findings likely indicate protein damage caused by the ^{18}F-FDG radiation, which was also described previously (34). However, these slight modifications on the ultrastructural level do not imply severe alterations of the cell's functionality or viability as shown here.

Labeling these stem cell types with ^{18}F-FDG therefore does not cause significant changes of cellular function in general, in comparison with groups that have been reporting direct cell labeling with other Food and Drug Administration–approved radiolabels with distinct side effects on certain cell types. Brenner et al. (35) have shown a decrease in cell viability, migration, and differentiation capacity after hematopoietic progenitor cells were labeled with 37 MBq

of ^{111}In-oxine per million cells. On the other hand, Aicher et al. (*36*) were not able to detect radiotoxic effects on endothelial progenitor cells after labeling with 15 MBq of ^{111}In-oxine per million cells.

Park et al. (*37*) have labeled rat MSCs with 264–1,057 MBq of ^{99m}Tc-hexamethylpropyleneamine oxime per million cells. This procedure did not affect cell viability; however, proliferation was decreased after labeling. Also, Detante et al. (*38*) could demonstrate a loss in colony-forming ability of cells labeled with ^{99m}Tc-hexamethylpropyleneamine oxime (53 MBq/million cells), but viability and proliferation were not influenced by the labeling procedure.

[111]In-oxine and ^{99m}Tc-hexamethylpropyleneamine oxime are isotopes that are typically used for SPECT. For direct labeling purposes with ^{18}F-FDG, a lower activity can be applied on the cells, because the sensitivity of PET is approximately one order of magnitude higher. Furthermore, these SPECT isotopes emit low-energy β^--particles. These particles will emit their radiation in a short range, thus inside the cells, causing a higher cellular toxicity.

Therefore, using radioisotopes for PET such as ^{18}F-FDG is a good option, because the resulting signal-to-noise ratio after labeling with lower activities is comparable to that of cells labeled with higher activities of typical SPECT radiotracer molecules.

These findings, together with our obtained results, demonstrate that the presence or absence of radiotoxic effects is rather cell type– and radiotracer-dependent. Therefore, our findings for ^{18}F-FDG cannot be transferred to other radiolabels or cell types.

To assess the in vivo biodistribution of labeled stem cells, small-animal PET images were acquired. The signal was mainly situated in the lungs, as expected because this is the first encountered capillary bed after intravenous injection. Cells will be trapped inside the pulmonary capillary network for a relatively long time after injection. These findings confirmed the intracellular location of the tracer.

Fifty-two percent and 43% of the injected activity was situated in the lungs for MSCs and MAPCs, respectively. The missing activity resulted from a combination of in vitro and in vivo elution of the ^{18}F-FDG taken up by the cells, as confirmed by dynamic small-animal PET data. The eluted tracer was determined to have been predominantly excreted through the urinary system, because the signal in the bladder gradually increased. The uptake of free ^{18}F-FDG molecules by the brain was low, as can be explained by the fact that the animals were already under anesthesia with isoflurane before injection of the labeled cells. The signal in the brain will therefore be low even if there is a significant washout of ^{18}F-FDG from the cells (*39*).

Moreover, it is important to consider the tissue and systemic effects of injecting radiolabeled cells into a subject. It is important to realize that the activities used for stem cell labeling (0.1–0.5 MBq for large animals or patients) are around 3 orders of magnitude lower than the ones used in clinical routine (~300 MBq for an adult weighing 75 kg; effective dose, ~6 mSv) and thus result in a clinically negligible effective dose range of 2–10 μSv. If one looks further on the organ level, we can assume that in a worst-case scenario 100% of the activity is within a single organ (e.g., lungs after intravenous injection, organ after injection in feeding artery) or concentrated at a single site (interstitial cell injection). This activity results in a concentration of 0.1 kBq/mL (e.g., 0.5 MBq retained 100% within the lungs) to 0.5 MBq/mL (e.g., 0.5 MBq retained in a 1-mL volume)—concentrations that are from 1 to 4 orders of magnitude lower than concentrations attained during clinical ^{18}F-FDG scans (e.g., 800 kBq/mL in normal lung and 8 MBq/mL in normal liver). Thus, even when all the activity of the labeled stem cells goes to a single organ or focus, the radiation dose to this organ is still much lower than the dose from a routine ^{18}F-FDG PET scan.

Comparing our data with the Hofmann et al. (*23*) clinical data, the injected activities are, however, within the same order of magnitude (0.04 MBq for our data vs. 0.12 MBq for the data of Hofmann et al.), in our opinion clearly demonstrating that the activity used for this labeling experiment can be translated to large-animal models and clinical patients.

CONCLUSION

In general, a generic method for direct stem cell labeling was optimized. ^{18}F-FDG labeling of MSCs and MAPCs did not perturb the biologic and functional properties of the cells. Furthermore, this labeling method permitted in vivo noninvasive early biodistribution studies using small-animal PET. This was the first time, to our knowledge, that ultrastructural changes were examined after radiolabeling in stem cells using TEM analysis. The assessment of ultrastructural changes caused by radiolabeling can reinforce and elucidate findings on the biologic and functional level. Therefore, this type of assessment can be useful in future optimizations of radiolabeling strategies.

DISCLOSURE

ACKNOWLEDGMENTS

REFERENCES

1. Shanthly N, Aruva MR, Zhang K, Mathew B, Thakur ML. Stem cells: a regenerative pharmaceutical. *Q J Nucl Med Mol Imaging.* 2006;50:205–216.

2. Weissman IL. Stem cells: units of development, units of regeneration, and units in evolution. *Cell.* 2000;100:157–168.

3. Friedenstein AJ, Gorskaja JF, Kulagina NN. Fibroblast precursors in normal and irradiated mouse hematopoietic organs. *Exp Hematol.* 1976;4:267–274.

4. Bosch P, Musgrave DS, Lee JY, et al. Osteoprogenitor cells within skeletal muscle. *J Orthop Res.* 2000;18:933–944.

5. Boquest AC, Shahdadfar A, Fronsdal K, et al. Isolation and transcription profiling of purified uncultured human stromal stem cells: alteration of gene expression after in vitro cell culture. *Mol Biol Cell.* 2005;16:1131–1141.

6. Gronthos S, Mankani M, Brahim J, Robey PG, Shi S. Postnatal human dental pulp stem cells (DPSCs) in vitro and in vivo. *Proc Natl Acad Sci USA.* 2000;97:13625–13630.

7. Caplan AI. Mesenchymal stem cells. *J Orthop Res.* 1991;9:641–650.

8. Pittenger MF, Mackay AM, Beck SC, et al. Multilineage potential of adult human mesenchymal stem cells. *Science.* 1999;284:143–147.

9. Uccelli A, Pistoia V, Moretta L. Mesenchymal stem cells: a new strategy for immunosuppression? *Trends Immunol.* 2007;28:219–226.

10. Jiang Y, Vaessen B, Lenvik T, Blackstad M, Reyes M, Verfaillie CM. Multipotent progenitor cells can be isolated from postnatal murine bone marrow, muscle, and brain. *Exp Hematol.* 2002;30:896–904.

11. Sohni A, Verfaillie CM. Multipotent adult progenitor cells. *Best Pract Res Clin Haematol.* 2011;24:3–11.

12. Subramanian K, Geraerts M, Pauwelyn KA, et al. Isolation procedure and characterization of multipotent adult progenitor cells from rat bone marrow. *Methods Mol Biol.* 2010;636:55–78.

13. Roobrouck VD, Clavel C, Jacobs SA, et al. Differentiation potential of human postnatal mesenchymal stem cells, mesoangioblasts, and multipotent adult progenitor cells reflected in their transcriptome and partially influenced by the culture conditions. *Stem Cells.* 2011;29:871–882.

14. Petite H, Viateau V, Bensaid W, et al. Tissue-engineered bone regeneration. *Nat Biotechnol.* 2000;18:959–963.

15. Zhou XZ, Leung VY, Dong QR, Cheung KM, Chan D, Lu WW. Mesenchymal stem cell-based repair of articular cartilage with polyglycolic acid-hydroxyapatite biphasic scaffold. *Int J Artif Organs.* 2008;31:480–489.

16. Badorff C, Brandes RP, Popp R, et al. Transdifferentiation of blood-derived human adult endothelial progenitor cells into functionally active cardiomyocytes. *Circulation.* 2003;107:1024–1032.

17. Nakamizo A, Marini F, Amano T, et al. Human bone marrow-derived mesenchymal stem cells in the treatment of gliomas. *Cancer Res.* 2005;65:3307–3318.

18. Miletic H, Fischer Y, Litwak S, et al. Bystander killing of malignant glioma by bone marrow-derived tumor-infiltrating progenitor cells expressing a suicide gene. *Mol Ther.* 2007;15:1373–1381.

19. Bengel FM. Noninvasive stem cell tracking. *J Nucl Cardiol.* 2011;18:966–973.

20. Caracó C, Aloj L, Chen LY, Chou JY, Eckelman WC. Cellular release of [^{18}F]2-fluoro-2-deoxyglucose as a function of the glucose-6-phosphatase enzyme system. *J Biol Chem.* 2000;275:18489–18494.

21. Prince HM, Wall DM, Ritchie D, et al. In vivo tracking of dendritic cells in patients with multiple myeloma. *J Immunother.* 2008;31:166–179.

22. Kang WJ, Kang HJ, Kim HS, Chung JK, Lee MC, Lee DS. Tissue distribution of ^{18}F-FDG-labeled peripheral hematopoietic stem cells after intracoronary administration in patients with myocardial infarction. *J Nucl Med.* 2006;47:1295–1301.

23. Hofmann M, Wollert KC, Meyer GP, et al. Monitoring of bone marrow cell homing into the infarcted human myocardium. *Circulation.* 2005;111:2198–2202.

24. Vidal MA, Kilroy GE, Johnson JR, Lopez MJ, Moore RM, Gimble JM. Cell growth characteristics and differentiation frequency of adherent equine bone marrow-derived mesenchymal stromal cells: adipogenic and osteogenic capacity. *Vet Surg.* 2006;35:601–610.

25. Bretschneider A, Burns W, Morrison A. "Pop-off" technic: the ultrastructure of paraffin-embedded sections. *Am J Clin Pathol.* 1981;76:450–453.

26. Doyle B, Kemp BJ, Chareonthaitawee P, et al. Dynamic tracking during intracoronary injection of ^{18}F-FDG-labeled progenitor cell therapy for acute myocardial infarction. *J Nucl Med.* 2007;48:1708–1714.

27. Melder RJ, Elmaleh D, Brownell AL, Brownell GL, Jain RK. A method for labeling cells for positron emission tomography (PET) studies. *J Immunol Methods.* 1994;175:79–87.

28. Adonai N, Nguyen KN, Walsh J, et al. Ex vivo cell labeling with ^{64}Cu-pyruvaldehyde-bis(N4-methylthiosemicarbazone) for imaging cell trafficking in mice with positron-emission tomography. *Proc Natl Acad Sci USA.* 2002;99:3030–3035.

29. Elhami E, Goertzen AL, Xiang B, et al. Viability and proliferation potential of adipose-derived stem cells following labeling with a positron-emitting radiotracer. *Eur J Nucl Med Mol Imaging.* 2011;38:1323–1334.

30. Chen MF, Lin CT, Chen WC, et al. The sensitivity of human mesenchymal stem cells to ionizing radiation. *Int J Radiat Oncol Biol Phys.* 2006;66:244–253.

31. Chan DC. Mitochondrial fusion and fission in mammals. *Annu Rev Cell Dev Biol.* 2006;22:79–99.

32. Detmer SA, Chan DC. Functions and dysfunctions of mitochondrial dynamics. *Nat Rev Mol Cell Biol.* 2007;8:870–879.

33. Ron D, Walter P. Signal integration in the endoplasmic reticulum unfolded protein response. *Nat Rev Mol Cell Biol.* 2007;8:519–529.

34. Daly MJ. Death by protein damage in irradiated cells. *DNA Repair (Amst).* 2012;11:12–21.

35. Brenner W, Aicher A, Eckey T, et al. ^{111}In-labeled CD34+ hematopoietic progenitor cells in a rat myocardial infarction model. *J Nucl Med.* 2004;45:512–518.

36. Aicher A, Brenner W, Zuhayra M, et al. Assessment of the tissue distribution of transplanted human endothelial progenitor cells by radioactive labeling. *Circulation.* 2003;107:2134–2139.

37. Park BN, Shim W, Lee G, et al. Early distribution of intravenously injected mesenchymal stem cells in rats with acute brain trauma evaluated by ^{99m}Tc-HMPAO labeling. *Nucl Med Biol.* 2011;38:1175–1182.

38. Detante O, Moisan A, Dimastromatteo J, et al. Intravenous administration of ^{99m}Tc-HMPAO-labeled human mesenchymal stem cells after stroke: in vivo imaging and biodistribution. *Cell Transplant.* 2009;18:1369–1379.

39. Toyama H, Ichise M, Liow JS, et al. Evaluation of anesthesia effects on [^{18}F]FDG uptake in mouse brain and heart using small animal PET. *Nucl Med Biol.* 2004;31:251–256.